CO4-1

Characterization of ion-irradiated yttria stabilized zirconia (YSZ) single crystal substrates using a slow positron beam

T. Ozaki, H. Sakane[1] and A. Yabuuchi[2]

School of Engineering, Kwansei Gakuin University
[1] *SHI-ATEX Co., Ltd.*
[2] *Institute for Integrated Radiation and Nuclear Science, Kyoto University*

INTRODUCTION: The rare-earth (RE)-based cuprate superconductor $REBa_2Cu_3O_y$ (REBCO) exhibits high in-field performance, and is expected to be useful for magnetic coils. Critical current properties in applied magnetic fields are enhanced by introducing structural defects using ion-irradiation techniques. Positrons are sensitive to vacancy-type defects, and they are useful for characterizing irradiation-induced defects. However, it is difficult to characterize irradiation-induced defects in GdBCO coated conductors (CCs), which were industrially produced with a roll-to-roll process because GdBCO CCs initially contain vacancy clusters, whose size is larger than that of the newly-formed defects induced by the irradiation [1]. In this study, we probed ion-irradiated yttria stabilized zirconia (YSZ), which is an oxidized material and almost the same density as GdBCO, single crystal substrates using a slow positron beam, so that we will evaluate the irradiation defect in these substrates using the positron annihilation measurement.

EXPERIMENTS: The YSZ single crystal substrates were irradiated with 600 keV He^+ or 10 MeV Au^{4+} ions. The unirradiated and irradiated samples were probed by the KUR slow positron beam and the Doppler broadening of annihilation radiation (DBAR) spectra were acquired with incident positron energies $E_+ = 9$ keV.

RESULTS: Figure 1 shows the positron lifetime spectra for the unirradiated and the irradiated YSZ single crystal substrates. We observed longer lifetimes of positron in the irradiated samples than that in the unirradiated sample. In addition, a longer lifetime component was clearly observed for the sample irradiated with 10 MeV Au-ions compared with that irradiated with 600 keV He-ions, suggesting that the size of lattice defects produced by 10 MeV Au-ions is larger than that produced by 600 keV He-ions.

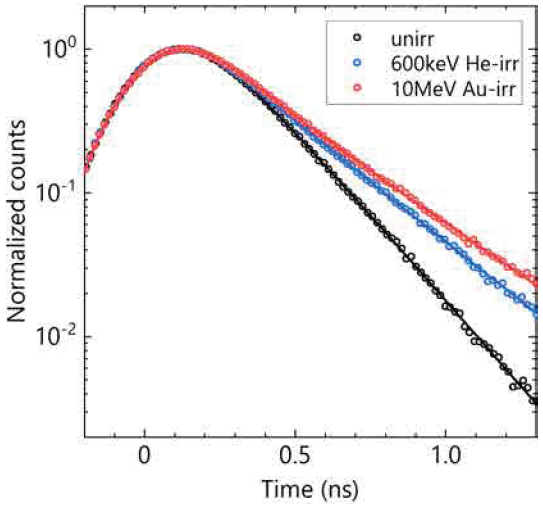

Fig. 1. Positron lifetime spectra for the unirradiated and the irradiated YSZ single crystal substrates.

REFERENCES:

[1] A. Yabuuchi *et al.,* Appl. Phys. Ex-press, **13** (2020) 123004.

CO4-2

Reducing Parasitic Scattering in Small-Angle X-Ray Scattering using Single Crystal Pinhole

Y. Oba, R. Inoue[1], K. Morishima[1] and M. Sugiyama[1]

Department of Mechanical Engineering, Toyohashi University of Technology
[1]Institute for Integrated Radiation and Nuclear Science, Kyoto University

INTRODUCTION: Small-angle X-ray scattering (SAXS) is a powerful tool for nanostructural characterization and used in a wide variety of research fields, such as polymer science, biology, and metallurgy [1,2]. To enhance the performance of SAXS, scatterless slit techniques have attracted attention [3-5]. They can drastically reduce parasitic scattering in X-ray collimation systems and allow efficient X-ray collimation. In this study, one of these techniques using single-crystal pinholes were applied to the SAXS instrument with Mo Kα radiation (Mo-SAXS) at the Institute for Integrated Radiation and Nuclear Science, Kyoto University.

EXPERIMENTS: SAXS experiments were carried out using Mo-SAXS (NANO-Viewer, Rigaku) with a conventional three-pinhole collimation system. Scattering patterns were measured using a photon-counting-type two-dimensional detector (PILATUS 100k, Dectris). The X-ray path from the X-ray entrance pinhole to the window just before the detector was evacuated to reduce the background scattering from air. The scattering patterns were reduced using our original program written in Igor Pro (WaveMetrics).

The single-crystal pinholes were made of tantalum discs with the thickness of 0.5 mm. A round hole with the diameter of 0.3-1.0 mm was opened at the center of each disc. In the current experiments, the two-pinhole collimation system was built using the normal X-ray entrance pinhole and the single-crystal pinhole just before the sample.

RESULTS: Fig. 1shows the comparison of the SAXS profiles between the conventional three-pinhole and new two-pinhole systems with the same primary beam size on the detector. The two-pinhole system provided almost 1/10 background intensity at $q < 0.15$ nm^{-1}, where q is the magnitude of the scattering vector. As the result, the data quality in this low q region was significantly improved and the practical low q limit reached 0.05 nm^{-1}. The background intensity in the high q region was also decreased. In addition, the incident X-ray intensity at the sample position increased 2.4 times.

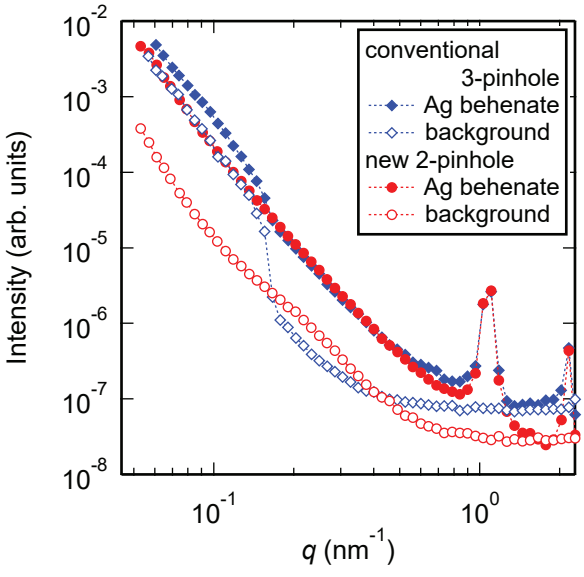

Fig. 1. SAXS profiles of background and Ag behenate obtained using conventional three-pinhole and new two-pinhole systems.

REFERENCES:

[1] Cy M. Jeffries *et al.,* Nat. Rev. Methods Primers, **1** (2021) 70.
[2] S. Da Vela, D. I. Svergun, Curr. Res. Struct. Biol., **2** (2020) 164.
[3] Y. Li *et al.,* J. Appl. Cryst., **41** (2008) 1134-1139.
[4] A. Schwamberger *et al.,* Nucl. Instrum. Met. Phys. Res. B, **343** (2015) 116-122.
[5] J. Lyngsø J. S. Pedersen, J. Appl. Cryst., **54** (2021) 295-305.

CO4-3

Neutron shielding performance of wood-based products

K. Murata[1], Y. Mimoto[1], M. Tsuchiya[2], K. Kariya[2], Y. Yamashiki[3], K. Takamiya[4]

[1]*Graduate School of Agriculture, Kyoto University*
[2]*Sumitomo Forestry Co., Ltd.*
[3]*Graduate School of Advanced Integrated Studies in Human Survivability, Kyoto University*
[4]*Institute for Integrated Radiation and Nuclear Science, Kyoto University*

INTRODUCTION: Neutron shielding is achieved using hydrogen-rich materials, such as water, polyethylene, and concrete, while elements with a large neutron absorption cross-section, such as boron, cadmium, and lithium, are used as absorbers. Because wood is primarily composed of carbon, oxygen, and hydrogen, and like polyethylene, is a hydrogen-rich compound, wood-based materials are also expected to exhibit good neutron shielding performance. In addition, fire-retardant wood products containing boron, which are commercially available, should have excellent neutron shielding performance. In this study, the neutron shielding performance of wood products was evaluated at a heavy water neutron irradiation facility (HWNIF) in the KUR.

EXPERIMENTS: The table 1 shows the materials prepared for neutron shielding test, which have a cross section of 80 mm × 80 mm and a thickness of 60 mm. Au foils and a cadmium-covered Au foils were placed in front of and behind the specimen, and the specimen was irradiated with mixed-mode neutron radiation in the HWNIF for 10 min. Gamma rays from the activated Au foils were measured using a Ge semiconductor detector, and shielding rates were obtained.

Table 1 Materials for estimating neutron shielding performance.

Symbol	Material	Symbol	Material
ASG	Air-dried sugi wood	FSG	Fire retardant sugi wood (boron)
DSG	Densified sugi wood	FPW	Fire retardant karamatsu plywood (boron)
WSG	Water impregnation sugi wood	PE	Polyethylene
KPW	Karamatsu plywood		

RESULTS: Fig. 1 shows a comparison of the neutron shielding rates of each product. Because PE and WSG have high shielding rates for epithermal neutrons, products rich in hydrogen atoms can effectively shield epithermal neutrons. However, because FSG and FPW have a high thermal-neutron shielding rate, it can be noted that elements with a large neutron absorption cross-section are effective in shielding thermal neutrons.

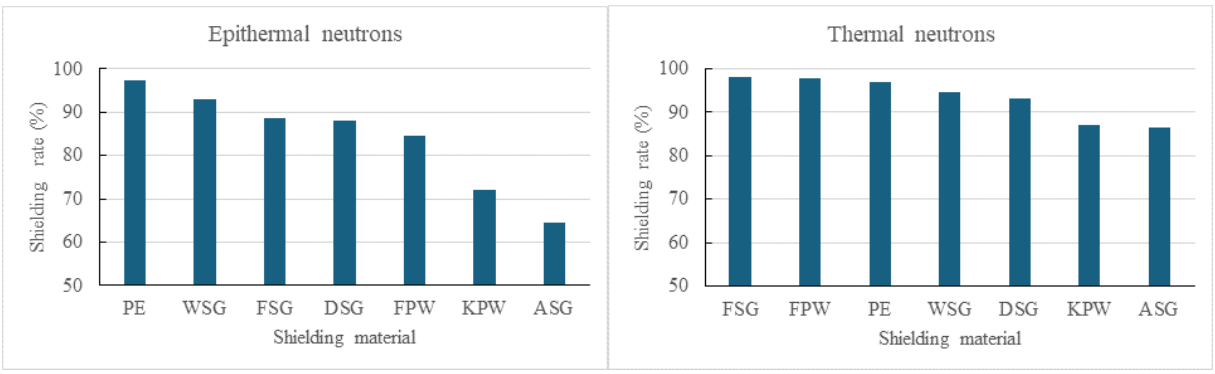

Fig. 1. Neutron shielding rates of wood products shown in Table 1.

CO4-4

Study on HPLC Elution Behavior of Heavy Lanthanide Metallofullerene Using Chlorobenzene Eluent

K. Akiyama, D. Nakamura, T. Kuroda, K. Takamiya[1], and S. Kubuki

Department of Chemistry, Tokyo Metropolitan University
[1]Institute for Integrated Radiation and Nuclear Science, Kyoto University

INTRODUCTION: Lanthanide (Ln) metallofullerene (EMF): Ln@C_{82} is a clathrate compound encapsulating metal atom in fullerene C_{82} and known that two or three electrons are transferred to C_{82} cage from the encapsulated Ln atom [1]. In the previous work, we succeeded to obtain the high-performance liquid chromatography (HPLC) elution behavior on a pyrenyl stationary phase for Ln@C_{82} of La, Ce, Pr, Nd, Gd, Tb, Dy, Ho, and Er with a toluene as an eluent by the thermal neutron activation method [2]. In this study, we used chlorobenzene (CB), which has a similar structure to toluene, as an eluent in order to obtain further knowledge about the HPLC elution behavior of Ln@C_{82}.

EXPERIMENTS: Ln@C_{82}s of Tb, Dy, and Ho were prepared by previously reported [2]. These purified samples were injected into a Buckyprep column using CB as an eluent. The eluate from the column was fractionated every 2 minutes at room Temperature (RT) and every 30 seconds at 50 ºC. These fractionated eluates were evaporated to dryness and re-dissolved to carbon disulfide and then dropped onto paper filters with 12 mm diameters and dried for 2 or 3 days in the evacuated desiccator. After sufficient drying, these samples were sealed into polyethylene bags and were activated by a thermal neutron in the KUR of the Institute for Integrated Radiation and Nuclear Science, Kyoto university. After the irradiation, the γ rays emitted from the samples were measured by a Ge detector.

RESULTS: Figure 1 shows HPLC chromatograms of Ln@C_{82} (Ln: Tb, Dy, Ho) using CB as a developing solvent at room temperature (left) and 50 oC (right). The retention times for each Ln@C_{82} were found to be 44.76 and 44.92 minutes for Dy, and Ho at room temperature and 40.73 minutes, 40.57 minutes, and 40.56 minutes for Tb, Dy, and Ho at 50 ºC. Although the retention time for Tb at room temperature is missing because accurate data was not available, adsorption desorption enthalpy for Dy and Ho were roughly estimated and found to be 3.5 and 3.6 kJ/mol for Dy and Ho respectively.

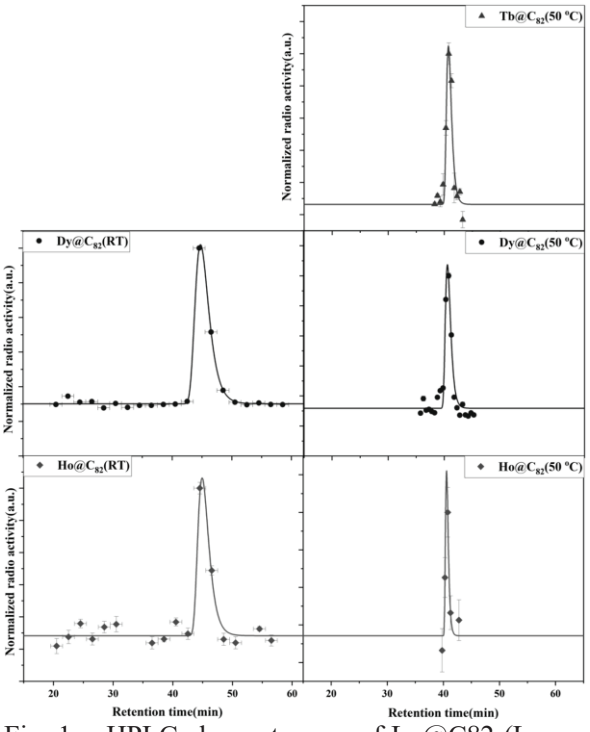

Fig. 1. HPLC chromatogram of Ln@C82 (Ln = Tb, Dy, and Ho) using CB as a developing solvent (left: room temperature, right: 50°C)

REFERENCES:

[1] H. Shinohara, Rep. Prog. Phys., **63** (2000) 843-892.
[2] K. Akiyama *et al.,* KURNS Prog. Rep. 2022 CO4-1.

CO4-5

Study on ^{99m}Tc separation/concentration technology from ^{99}Mo by (n, γ) method (3)

H. Suematsu, Y. Yang, T. Kitagawa, T. M. D. Do, T. Suzuki, Y. Fujita[1], Y. Fujihara[2], H. Yoshinaga[2] and J. Hori[2]

Graduate School of Engineering, Nagaoka University of Technology
[1]Fuels and Materials Department, Japan Atomic Energy Agency
[2]Institute for Integrated Radiation and Nuclear Science, Kyoto University

INTRODUCTION: ^{99}Mo production methods by neutron irradiation of MoO_3 targets were studied and an effective extraction method using ^{99}Mo hot atoms was developed[1]. In the former research, β-MoO_3 whiskers were used as the neutron irradiation targets[1]. However, it was not certain whether the high extraction rate was caused by the short diffusion path of ^{99}Mo in the whisker or the wide spacing of MoO_5 pyramids in the β-MoO_3 crystal. Furthermore, α-MoO_3 was also present in the target. In this work, high purity β-MoO_3 particles were synthesized by a thermal evaporation method using a metal filter to separate large α-MoO_3 crystals from fine β-MoO_3 particles for the neutron irradiation and ^{99}Mo extraction experiments.

EXPERIMENTS: α-MoO_3 powder was placed in a tube furnace heated at 900 ºC in flowing O_2 gas at 60 kPa with a flow rate of 8L/min. In the downstream side of the furnace, a # 500 metal filter was placed to catch large α-MoO_3 crystals. Then fine β-MoO_3 particles were collected on a membrane filter. The β-MoO_3 particles were irradiated by neutrons in KUR at $3x10^{13}$ n/cm^{2}s for 20 min. The irradiated particles (solid sample) was dispersed in water at room temperature up to 24 hour. The irradiated particles were separated by a centrifuge and a membrane filter to prepare solution sample. The activities of solid and solution samples were measured by a Ge detector were used to estimate the extraction rate of ^{99}Mo from the solid to solution samples.

RESULTS: Scanning electron microscopy (SEM) image of the β-MoO_3 particles is shown in Fig. 1. From the image, the geometric mean diameter was measured to be 130 nm. The time dependence of extraction rate is shown in Fig. 2. 75% of the formed ^{99}Mo in β-MoO_3 particles by the neutron irradiation was successfully extracted even at room temperature. From these experiments, it was concluded that β-MoO_3 particles can work as a target to produce and extract ^{99}Mo in water.

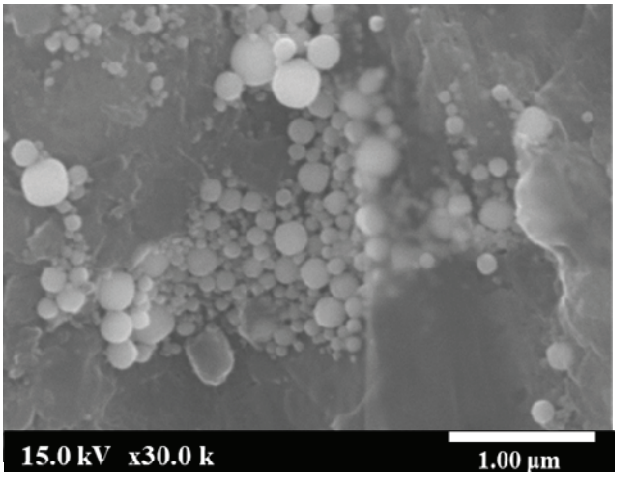

Fig. 1. SEM image of β-MoO_3 particles

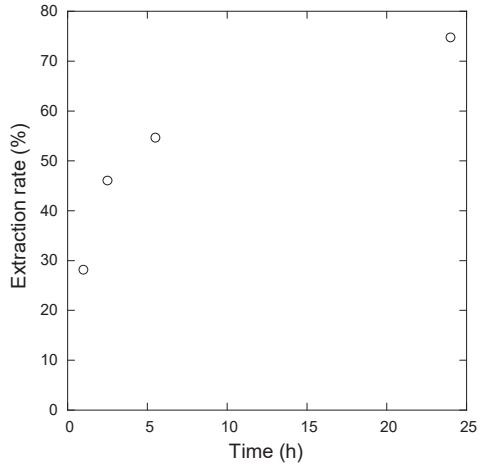

Fig. 2. Extraction rate of ^{99}Mo to water

REFERENCES:

[1] M. C. Ngo *et al.,* Inorganic Chem., **62** (2023) 131040.

CO4-6

Complex Structure of Ions Coordinated with Hydrophilic Polymer 25. Examination for "Diffusion-induced Orientation" Observed in PA6 Considering Dynamic Structure of Polyiodides.

A. Kawaguchi , A. Kita, Y. Morimoto

IIRNS, Kyoto University (KURNS)

INTRODUCTION: We have been investigating dynamical and interacted structures between iodine and polymers. Here, "iodine" is mentioned containing "polyiodide ions" (I_n^{m-}, m, n: integer, n > 1: "Poly-Iod." mentioned below), which are defined as charged molecules constructed with more than one iodine atom. And, Poly-Iod.(s), mono iodide ion (I^-) and iodine (I_2) can actively interact with each other as molecular (re)structuring between (or among) them originated by "halogen (iodine) bonding". Such structured iodine arrays can be often observed in coordination within organic crystals.[1] And interaction and structuring are more emphasized through coordination with macromolecular matrices as both hydrophilic and hydrophobic polymers.

Interaction and (re)structuring among Poly-Iod., I^-, and I_2 are characterized by "charge conjugation" and "iodine bonding", which is loose and anisotropic; it means that iodine arrays behave as "pseudo polymer" under charge shearing. And, polyamide 6 (PA6) is one of hydrophilic polymers showing active interaction with Poly-Iod. Additionally, PA6 is crystalline polymer and is induced phase transition through coordination with Poly-Iod.[2]

EXPERIMENTS: As starting PA6, non-oriented film ("Rayfan^{TM}", 100μm in thickness) provided by TORAY was prepared. And, while "non-oriented PA6" was annealed without stretching, "doubly oriented PA6" was annealed after stretched keeping filmy form. They were doped in 0.1N I_2-KI(aq) at 5deg. (iodine doping).

RESULTS AND DISCUSSION: After "iodine doping", (1) "non-oriented PA6" without chain orientation by stretching showed formation of chain axis normal to filmy surface of the sample. On the other hand, (2) "doubly oriented PA6" with chain orientation (c-axis of PA6 α-crystal) by stretching showed both "parallel orientation (to film surface)" of bc-plane of the crystal and "normal orientation (to film surface)" of the bc-plane while chain orientation (c-axis) was maintained before and after doping.[3] These results indicate that dynamic modification of chain orientation and crystalline axes (or maintenance for some of them) advance on iodine doping for PA6, but that not only diffusion of Poly-Iod. into matrices but their coordination with host polymer are implemented in structure anisotropy.

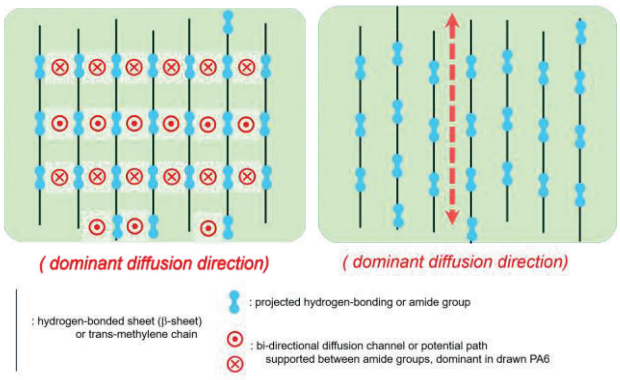

Then, "modified orientation" reported previously should also be explained by such dynamism; hypothesized "dynamic amphiphilicity" which guarantees self-organization can explain both diffusion and coordination of Poly-Iod.'s normal and parallel to chain axis. While driving force originated "iodine bonding" enables normal orientation of chains (Fig; right) to non-oriented sample surface, it performs normal and bi-directional diffusion normal to chains in doubly oriented sample. (Fig; left) Such scheme may suggest that diffusion of Poly-Iod.'s and charge conjugation along them are constructed both parallel and normal to chain axis as self-organized (modified) structure.[4]

REFERENCES:

[1] T.J. Marks & D.W. Kalina, "Extended Linear Chain Compounds" vol.1 ch.6., ed. J.S. Miller (Plenum Press, 1982).
[2] H. Arimoto, J. Polym. Sci. A, **3** (1964), 2283-2295.
[3] A. Kawaguchi, Polymer, **35** (1994) 3797-3798.
[4] A. Kawaguchi, Polym. Prep. Jpn., **71** (2022) 1J-20.

R6063

CO4-7

Research and Develop of M/HEA as Structure Materials For Nuclear Reactor

N. Hashimoto, K. Saito[1], H. Oka

Department of Materials Science and Engineering, Hokkaido University, Sapporo 060-8628
[1]Graduate Student, Graduate School of Engineering, Hokkaido University, Sapporo 060-8628

INTRODUCTION: To investigate the effect of compositional complexity on the microstructural evolution, the face-centered cubic (fcc) Medium Entropy Aloys were electropolished, and thin-foil samples were prepared for in-situ electron irradiation experiments at Hokkaido University. Electron-irradiated bulk samples were also prepared at the Institute for Integrated Radiation and Nuclear Science, Kyoto University, for the positron annihilation spectroscopy (PAS) at the International Research Center for Nuclear Materials of the Institute of Materials Research (IMR), Tohoku University. (MEAs), CrFeNiMn-type HEAs and a CrFeNi ternary alloy, were subjected to e^- irradiation.

EXPERIMENTS: $Cr_{0.8}FeMn_xNi$ (x = 0.4, 1.0, 1.5) alloys and CrFeNi were prepared by arc-melting and subjected to homogenization heat treatment (1160℃, 24h), cold-rolling (90%), and recrystallization heat treatment (1000℃, 4h) to prepare the test materials. Electrolytic polishing was used to prepare thin films for electron microscope observation, and the formation and growth process of dislocation loops were observed by electron beam irradiation experiments using a high-voltage electron microscope. The growth rate of the obtained dislocation loops and the supersaturation number density were organized as a function of temperature to measure the vacancy and interstitial migration energy. Additionally, after e^- beam irradiation of the bulk samples, positron annihilation measurements were performed to calculate the migration energy of atomic vacancies.

RESULTS: The migration energy of vacancies can be determined by measuring the lifetime of positrons introduced into an alloy (positron lifetime method). The vacancy concentration in an alloy is calculated by measuring the time it takes for a positron to be captured by an electron and annihilated, taking advantage of the property that the electron density is relatively low around the vacancies. In this study, the change in the residual vacancy ratio in an annealed sample was experimentally investigated, and the vacancy migration energy was selected so that the calculated value (by means of the equation as bilow) of the residual vacancy ratio was most consistent.
First, the positron lifetimes of the unirradiated and irradiated alloys were 106.7±0.5 (ps) and 146.1±0.2 (ps), respectively, confirming that atomic vacancies were introduced into the alloy by electron beam irradiation. Fig. 1 shows the annealing temperature dependence on positron lifetime in CrFeNi and $Cr_{0.8}FeMnNi$. In this experiment, the migration energies of vacancies in CrFeNi and $Cr_{0.8}FeMnNi$ were similar, suggesting that there was no significant change in the microstructural change due to irradiation damage. This result differs from the findings obtained from a separate in-situ electron beam irradiation experiment, and it was confirmed once again that it is not easy to calculate the vacancy migration energy by experiment. Furthermore, previous research has shown that the mobility of point defects is strongly affected by the impurity concentration in the alloy, reaffirming the need for further precise experiments in the future.

ACKOWLEDGEMENT: This study was supported by the Institute of Integrated Radiation and Nuclear Science, Kyoto University, for the electron irradiation experiment and the Institute for Materials Research, Tohoku University for the positron lifetime measurement experiment.

REFERENCES: [1] Z. Zhang *et al.* Progress in Materials Science 123, (2022), 100807.
[2] Dusadi., Computational Materials Science 237, (2024), 112912.

CO4-8

Neutron shielding and activation characteristics of novel iron oxide ceramics

H. Terato, and Y. Sakurai[1]

Advanced Science Research Center, Okayama University
[1]Institute for Integrated Radiation and Nuclear Science, Kyoto University

INTRODUCTION: Shielding is an essential procedure in the handling of ionizing radiation and radioisotopes. Shielding materials must be appropriately selected based on the type and energy of the radiation. Lead blocks are commonly used to shield gamma rays and X-rays; however, due to the toxicity of lead, there is a global trend toward avoiding its use. We have developed a novel iron oxide-based ceramic and evaluated its gamma-ray shielding capability, demonstrating its potential as a gamma-ray shielding material [1]. Furthermore, shielding materials used in reactor and accelerator facilities must also be evaluated for their effectiveness against neutrons and their activation characteristics. In this study, we evaluate the neutron shielding performance and activation behavior of the developed material using reactor neutrons. Additionally, we assess the generation of secondary gamma rays (prompt gamma rays) induced by neutron irradiation.

EXPERIMENTS: The neutron shielding effectiveness was evaluated using the carrying system of Heavy Water Neutron Irradiation Facility (HWNIF). The shielding performance of iron oxide ceramics with varying thicknesses was assessed using activation foils, such as gold foils. In this experiment, samples measuring 10 cm × 10 cm with a thickness of 1 cm were prepared and used in stacked configuration. The experiment was conducted at 1 MW for approximately 3 hours. To evaluate the activation characteristics, additional experiments were performed using the rail system of HWNIF. Iron oxide ceramic samples measuring 2 cm × 2 cm with a thickness of 1 cm were irradiated for approximately 5 or 50 minutes, and their activation was analyzed using an HPGe semiconductor detector. The experiment was also conducted at 1 MW for about 3 hours. To investigate the characteristics of prompt gamma-ray generation, experiments were conducted using the prompt gamma-ray analysis (PGA) system installed in Neutron Guide Tube (E-3). Iron oxide ceramic samples measuring 2 cm × 2 cm with a thickness of 1 cm were used, and the experiment was carried out at 1 MW for approximately 5 hours. In all experiments, control tests were also performed using iron and lead samples of the same dimensions as the iron oxide ceramics for comparison.

RESULTS: The thermal neutron shielding performance of the iron oxide ceramics was found to be intermediate between that of lead and iron, while the shielding performance against epithermal neutrons was closer to that of lead than to iron. In other words, the material demonstrated better neutron shielding than lead but was inferior to iron. As the gamma-ray shielding ability of ceramics and iron is generally proportional to their densities, similar results were observed in this aspect. Therefore, within the required shielding performance range, the ceramics are expected to offer a weight-reduction advantage. The characteristics of secondary gamma-ray generation in the ceramics were found to be nearly equivalent to those of iron. For thermal neutrons, the observed values were more than an order of magnitude higher than those of lead, mainly due to the (n,γ) reactions of iron. Regarding activation, the induced radioactivity ratio was approximately iron : ceramics : lead = 20 : 1 : 0.00003. This is primarily attributed to the generation of Mn-56 from iron. These results indicate that while the ceramics possess a certain level of neutron shielding capability, additional measures are required to address issues related to secondary gamma-ray generation and activation.

REFERENCES:
[1] M. Isobe *et al.,* Radiat. Safety Management, **22** (2023) 1-6.

CO4-9

Radiation Properties of Wide-bandgap Semiconductor Sensors for High-Energy Physics Experiments

T. Kishishita, H. Yashima[1], Y. Sakurai[1], R. Kosugi[2], T. Nakano[3,4], R. Kudo[4], T. Sakurai[4], Y. Hashimoto[4]

High Energy Accelerator Research Organization, KEK
[1] Institute for Integrated Radiation and Nuclear Science, Kyoto University
[2] National Institute of Advanced Industrial Science and Technology
[3]Department of Electronics and Materials Science, Shizuoka University
[4]Research Institute of Electronics, Shizuoka University

INTRODUCTION: Wide-bandgap semiconductor sensors have been considered as a potential alternative to Si for the manufacture of dosimeters, spectrometers, and charge particle detectors in high energy physics experiments, by virtue of its operation capability in strong radiation and/or high-temperature environments. To take advantage of such properties for future radiation detectors with a comparable size of silicon, we investigated two different semiconductor materials, SiC and BGaN this year. This study focuses on the influence of the SiC's bulk defects on the radiation sensor characteristics under the reverse-bias condition and neutron-detectability with BGaN sensors, by irradiating neutrons at Institute for Integrated Radiation and Nuclear Science, Kyoto University.

EXPERIMENTS: The reverse blocking characteristics and leakage current characteristic are primary concerns of the radiation effects on SiC. On the other hand, BGaN, a mixed semiconductor of GaN and BN, is expected to be a novel neutron detection material because it contains boron (B), a neutron-capturing element, as a semiconductor constituent. Therefore, we conducted different measurements with each sensor. As for the SiC sensor, we irradiated fast neutrons to SiC pn-diodes under the bias condition of 1 kV [1]. Fig. 1 shows the photograph of the measurement setup. We installed two SiC sensors at the front of the rail-instrument. After the 1MW operation, we carried out measurements of the leakage current and compared with those of the pre-irradiation samples. As for the BGaN, the sensor signals have been taken during the irradiation by external DAQ system and signal amplitudes and rise times were evaluated in off-line. The irradiation tests were both conducted at KUR.

RESULTS: The typical I-V characteristics of SiC sensors before and after irradiation showed similar characteristics, and we did not observe any degradation in leakage currents after the irradiation of 1E+12 n_{eq}/cm^2 fluence. The reverse blocking property was also retained up to 1 kV, which is required for full depletion of the SiC devices. We also conducted the Slant-irradation test for 4 hours for higher fluence, however, the device was heavily radio-activated, and thus, we could not measure the I-V characteristics. According to those results, we are currently developing a prototype muon beam monitor for the COMET experiment. The preliminary result was published in Ref. [1]. We will cotinue the measurement in 2025. As for the BGaN sensors, neutron-detectability was confirmed with sufficient event rates.

Fig. 1. Photograph of the measurement setup.

REFERENCES:

[1] T. Kishishita *et al.,* "Prototype of SiC beam monitor for the COMET experiment at J-PARC", JINST 20 (2025) C02016.
[2] K. K. Lee *et al.,* Nucl. Instrum. Methods Phys. Res. B, **210** (2003) 489-494,

CO4-10

Influence of Hydrogen Isotopes on Growth of Vacancy Clusters in Tungsten-Based Materials

Y. Hatano, E. Taguchi, A. Matsumoto, K. Fukuda[1], T. Takahashi[2], N. Abe[2] and A. Kinomura[2]

Graduate School of Engineering, Tohoku University
[1]Guraduate School of Science and Engineering, University of Toyama
[2]Institute for Integrated Radiation and Nuclear Science, Kyoto University

INTRODUCTION: As a plasma-facing material of a fusion reactor, tungsten (W) will be exposed to fuel particles, deuterium (D) and tritium (T), and products of fusion reactions, helium and 14 MeV neutrons. Vacancies and vacancy clusters formed by neutron irradiation act as strong traps against hydrogen isotopes and increase T inventory in W [1]. Understanding of vacancy formation and clustering is necessary for accurate evaluation of T inventory in a vacuum vessel of a fusion reactor. Displacements by neutrons occur under exposure to hydrogen isotope plasma, and hence hydrogen isotopes may affect the growth and decomposition of vacancy clusters.
The objective of this study is to investigate the influence of hydrogen isotopes on behaviors of vacancy and vacancy clusters to construct a kinetic model of clustering and annihilation. To reach this goal, W samples with monovacancies and vacancy clusters are prepared by electron beam irradiation. Then, the irradiated samples are heated with and without hydrogen isotopes, and the difference in size distributions of vacancy clusters is examined using positron annihilation spectroscopy.
****

EXPERIMENTS: Disk samples of W were irradiated with 8 MeV electrons using KURNS-LINAC to 10^{-3} displacement per atom (dpa). A part of irradiated samples was exposed to D atoms at 200 ℃ to introduce D atoms and then heated under D_2 gas atmosphere at 0.1 MPa and 400 ℃ for 20–40 h. The other part of samples without D atoms were also heated at 400 ℃ for 20–40 h in vacuum. Positron lifetime was measured by using ^{22}Na source at Institute for Materials Research, Tohoku University [1].
****

RESULTS: The positron lifetime was 143 ps before the irradiation. As summarized in Fig. 1, the electron beam irradiation resulted in the generation of long-life components around 363 ps which is attributable to the formation of vacancy cluster [2]. The exposure to D atoms reduced the long-life component to 329 ps. This is because each trapped D atom brought 1 electron into a vacancy cluster. Subsequent annealing at 400 ℃ in vacuum led to shorter in long-life component. This observation can be ascribed to reduction in vacancy cluster size due to decomposition. The sample annealed under the presence of D atoms systematically showed larger values of long-life component than that annealed in vacuum. These observations suggest that D atoms hindered the decomposition of vacancy clusters.
****

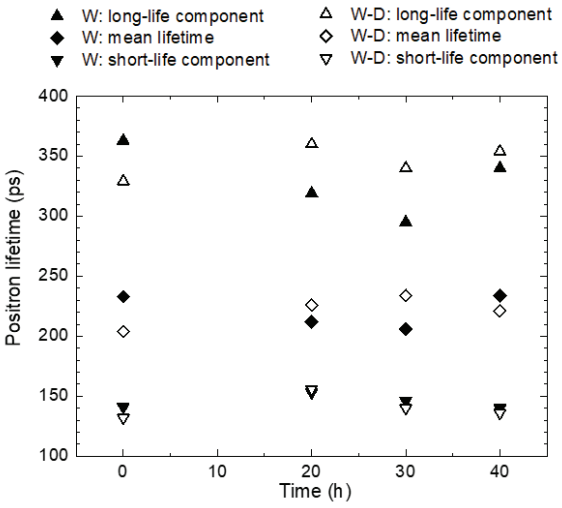

Fig. 1. Positron lifetime of electron irradiated W after annealing at 400 ℃ with and without deuterium (D).

REFERENCES:

[1] T. Toyama *et al.,* J. Nucl. Mater., **499** (2018) 464.
[2] T. Troev *et al.,* Nucl, Instr. Meth. B, **267** (2009) 535.

CO4-11

Structural Response of Guar-gum Hydrogels to Temperature via Small Angle X-ray Scattering

T. Tominaga, R. Inoue[1], and M. Sugiyama[1]

Neutron Science and Technology Center, Comprehensive Research Organization for Science and Society (CROSS)
[1]Institute for Integrated Radiation and Nuclear Science, Kyoto University

INTRODUCTION: Soft matter is characterized by its ability to undergo large deformation. A hydrogel is a soft material capable of extensive deformation [1]. Furthermore, additives can either enhance or inhibit its mechanical properties of the hydrogels. Guar-gum (GG) hydrogels can achieve significantly greater deformation when proper amounts of borax (cross-linker, Bx), glycerin (Gly), and vinyl acetate resin particles (Bd) are added, compared to GG gels containing only borax.
Previous small-angle X-ray scattering (SAXS) analysis of the hydrogels prepared from GG with the incorporation of Bx, Gly, and particles revealed that Gly mainly contributed to the structural homogenization, whereas Bx and Bd induced the structural inhomogeneity [2]. Structural changes during the elongation process of slime could not be evaluated due to extremely rapid relaxation. In this study, the influence of individual additives on temperature-dependent behavior was assessed through measurement of thermal responses in the internal structure of the hydrogel specimens utilizing SAXS.

EXPERIMENTS: GG hydrogels were synthesized with the following weight ratios: GG (2–3 wt.%), Gly (7 mL), Bx (0.4 g), Bd (2–3 g), and water (88 g). The samples were sandwiched between polyetherimide film (0.5 mm, Sperio, Mitsubishi, Japan). Cu-SAXS (RIGAKU Nanopix) in high-resolution mode was conducted at the Institute for Integrated Radiation and Nuclear Science, Kyoto University. The sample temperature was varied from 15–55°C using a Peltier temperature control system. The empty cell correction was applied to account for transmission, and the scattering profile, I(Q), was obtained via circular averaging.

RESULTS: SAXS profiles of GG hydrogels are shown in Figure 1. The top panel represents GG + Bx + Bd, while the bottom shows GG + Gly + Bx + Bd. Without Gly, high Q scattering intensity increased with temperature, whereas with Gly, the slope at $Q < 0.1$ Å^{-1} decreased, showing the suppression of temperature dependency of hydrogel.
Bx forms cross-links, introducing structural irregularities, while Gly reduces heterogeneity by enhancing fluidity near GG chains. The internal structures at $Q < 0.02$ Å^{-1} depend on resin on the other hand, it remains stable regardless of temperature change. Because Gly and Bx affect the opposing structural features, their ratio, distribution relative to GG, and respective functions could tend to contribute significantly to the slime's mechanical properties.
We plan to analyze the data with and without other additives and combine them in an original paper.

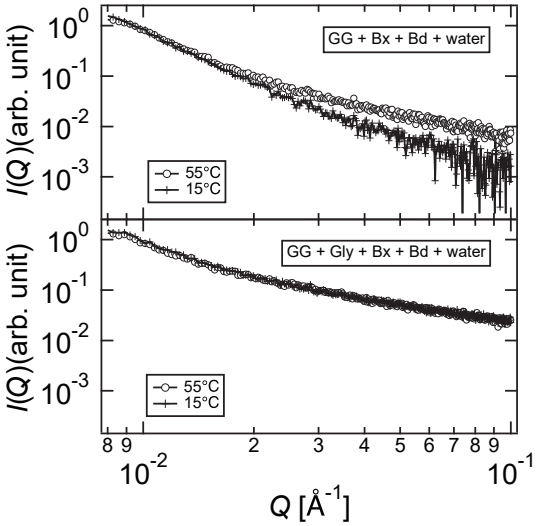

Fig. 1. Temperature dependence of SAXS profiles of GG + Bx + Bd + water hydrogel (top) and, GG + Gly + Bx + Bd + water hydrogel (bottom).

REFERENCES:
[1] T. Kanaya *et al.,* Polymer Journal, **44** (2012) 83–94.
[2] T. Tominaga *et al.,* KURNS Progress Report 2022, CO4-14 (2022) 105.

CO4-12

Thermal Behavior of Vacancies and Absorbed Hydrogen Atoms in Palladium Metal

W. Sato, M. Furumoto[1], Y. Shimizu[1], H. Shimizu[2], Y. Ohkubo[3] and A. Taniguchi[3]

Institute of Science and Engineering, Kanazawa University

[1]Graduate School of Natural Science and Technology, Kanazawa University
[2]Nishina Center for Accelerator-Based Science, RIKEN
[3]Institute for Integrated Radiation and Nuclear Science, Kyoto University

INTRODUCTION: Palladium (Pd) can occlude a large amount of hydrogen in the lattice interstitial sites; thus the metal is expected to be applied in industry as hydrogen storage material. However, the occlusion of hydrogen is likely to induce the formation of lattice defects, which causes the deterioration of its storage performance. Such a problem could be an obstacle to its practi-cal uses. In order to realize high performance of hydrogen occlusion in Pd, therefore, it is im-portant to understand the characteristics of the hydrogen-induced lattice defects as well as the ther-mal behavior of hydrogen impurities themselves in Pd [1]. In the present work, we have obtained atomic level information on those defects using two different nuclear spectroscopic techniques: positron annihilation lifetime spectroscopy (PALS) and perturbed angular correlation (PAC) spectroscopy.

EXPERIMENTS: A commercially available Pd plate of a purity of 99.95% was irradiated with thermal neutrons in the research reactor of Kyoto University (KUR) to produce the ^{111}Cd($\leftarrow^{111}$Ag$\leftarrow^{111}$m, ^{111}Pd) probe, and TDPAC measurements were performed by the detection of the 97-245 keV cascade γ rays with the intermediate level of I = 5/2 having a half life of 85.0 ns. Apart from the PAC experiment, PALS measurements with a positron source of ^{22}Na were performed for a pristine and hydrogen-absorbed/desorbed Pd at room temperature. The PALS spectra were analyzed with a fitting program PALSfit [2]. For the absorption of hydrogen atoms into Pd lattice, we adopted an electrochemical method [3].

RESULTS: PALS measurements disclosed the effect of hydrogen occlusion on the local structure in the Pd lattice, suggesting the formation of dislocation and open-volume defects. It was also found that heat-treatments at 383 K thoroughly evacuate the absorbed hydrogen from the lattice of Pd. PAC spectroscopy with the ^{111}Cd probe revealed temperature-dependent dynamic behavior of hydrogen atoms as shown by the exponential relaxation of the PAC spectra in Fig. 1, and the spectral analyses have shown that the activation energy of their thermal motion is 47(3) meV.

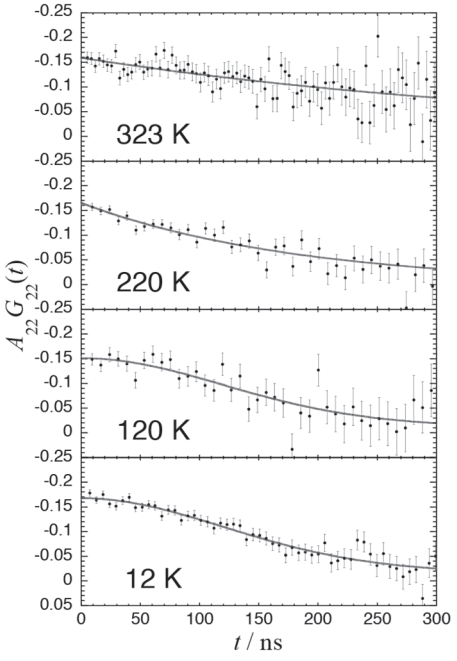

Fig. 1. Temperature-dependent TDPAC spectra of the ^{111}Cd($\leftarrow^{111}$Ag$\leftarrow^{111m,\ 111}$Pd) probe in a hydrogen-absorbed Pd plate.

REFERENCES:

[1] M. Mihara *et al.,* JPS Conf. Proc., **21** (2018) 011031.
[2] J. V. Olsen *et al.,* Phys. Status Solidi C, **4** (2007) 4004-4006.
[3] W. Sato *et al.,* J. Appl. Phys., **135** (2024) 245103.

CO4-13

Investigation of Temperature-Dependent Cd Dopant Sites in $Cd_{0.2}Sr_{0.8}TiO_3$ Studied by TDPAC Spectroscopy

S. Komatsuda, W. Sato[1], A. Taniguchi[2], M. Tanigaki[2], and Y. Ohkubo[2]

Institute of Human and Social Sciences, Kanazawa University
[1]*Institute of Science and Engineering, Kanazawa University*
[2]*Institute for Integrated Radiation and Nuclear Science, Kyoto University*

INTRODUCTION: $SrTiO_3$ is one of the most promising candidates for photocatalytic materials. It is known that trivalent cation doping at the Ti^{4+} site is one of the effective methods to improve photocatalytic activity. According to our previous research, it was suggested that the doped In contributed to the improvement of the photocatalytic activity by substituting Ti[1]. Furthermore, it was found from our other experiments that Cd^{2+} occupies the same Ti^{4+} site as In^{3+} in $Cd_xSr_{1-x}TiO_3$ perovskite structure at high Cd concentrations ($0.06 \leqq x \leqq 0.20$). For a practical use of $Cd_xSr_{1-x}TiO_3$, it is necessary to obtain microscopic information on impurity sites at various temperatures. Therefore, for the microscopic study of the local fields at Cd sites, the TDPAC measurements were performed for ^{111}Cd($\leftarrow^{111m}$Cd) in $Cd_{0.2}Sr_{0.80}TiO_3$ at room temperature and at 500 K.

EXPERIMENTS: Stoichiometric amount of $SrCO_3$, $CdCO_3$, and TiO_2 powders was mixed in a mortar. The powders were pressed into disks. For TDPAC measurements, about 3 mg of CdO enriched with ^{110}Cd was irradiated with thermal neutrons at Kyoto University Research Reactor, and radioactive ^{111m}Cd was generated by the ^{110}Cd(n, γ)^{111m}Cd reaction. The neutron-irradiated CdO powder was dissolved in 6M HCl and added in droplets onto the pre-sintered $Cd_{0.2}Sr_{0.80}TiO_3$ disk. The disk was sintered in air at 1373 K for 90 min. TDPAC measurements were carried out for the 151-245 keV cascade γ rays of ^{111}Cd($\leftarrow^{111m}$Cd) probe with the intermediate state of $I = 5/2$ having a half-life of 85.0 ns.

RESULTS: Figure 1 shows the TDPAC spectra of the ^{111}Cd($\leftarrow^{111m}$Cd) probe embedded in $Cd_{0.2}Sr_{0.80}TiO_3$ at room temperature and at 500 K. From the fitting parameters of TDPAC spectra in Fig. 1, spectral patterns can be reproduced by a fit with unique quadrupole frequencies. It is suggested from our previous study that Cd dopants replace Ti^{4+} in the lattice sites where defect exists in the vicinity of the Cd probes[1]. The value of the electric quadrupole frequency decreased slightly at 500 K, suggesting that the lattice expanded at 500 K. No other significant differences were observed in the spectra of the two, which suggests that the local structure around Cd remains stable at high temperatures. For more information on temperature dependence, TDPAC measurements of $Cd_xSr_{1-x}TiO_3$ perovskite at 500~100 K are now in progress.

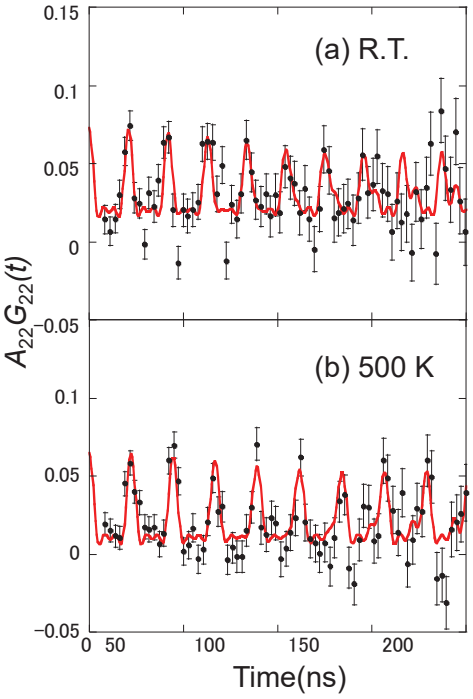

Fig. 1. TDPAC spectra of ^{111}Cd($\leftarrow^{111m}$Cd) in $Cd_{0.2}Sr_{0.80}TiO_3$ (a) at room temperatures and (b) at 500 K.

REFERENCES:

[1] S. Komatsuda *et al.*, Interactions, **245** (2024) 37.

CO4-14

Investigation of the Dynamics of Rigid Helical Polymers via Small-Angle X-Ray Scattering, Dynamic Light Scattering, and Molecular Dynamics Simulations

Y. Nagata[1], M. Sugiyama[2], R. Inoue[2], N. Sato[2], and K. Morishima[2]

[1] *Institute for Chemical Reaction Design and Discovery, Hokkaido University*
[2]*Institute for Integrated Radiation and Nuclear Science, Kyoto University*

INTRODUCTION: Poly(quinoxaline-2,3-diyl)s (PQXs) represent a novel macromolecular scaffold that exhibits solvent-induced switching of helical chirality. For instance, a 100-mer PQX bearing (R)-2-octyloxymethyl side chains (**2oct**) adopts distinct helical conformations: a right-handed (P-helical) structure in tetrahydrofuran (THF) and a left-handed (M-helical) structure in a 4:1 (v/v) mixture of 1,1,2-trichloroethane (1,1,2-TCE) and THF. [1]

To elucidate the mechanism underlying the solvent-dependent helix inversion of **2oct**, both experimental and theoretical investigations have been conducted. Small-angle neutron scattering (SANS) studies revealed differences in the spatial arrangement of the side chains relative to the main chain in THF-d_8 and 1,1,2-TCE-d_3/THF-d_8. [2] Furthermore, quasielastic neutron scattering (QENS) directly probed the side-chain dynamics of **2oct** in these solvents. By combining QENS results with molecular dynamics (MD) simulations, a coupling between main-chain and side-chain dynamics was uncovered, suggesting that differences in side-chain mobility may drive the switching of helical chirality. [3]

Remarkably, solvent-dependent helix inversion has also been observed in PQXs dissolved in simple saturated hydrocarbon solvents. A PQX bearing (S)-3-octyloxymethyl side chains demonstrates a pronounced solvent effect, undergoing helix inversion from an M-helical structure in n-octane to a P-helical structure in cyclooctane. The efficiency of this solvent effect, induced purely by switching between alkane solvents, is particularly noteworthy. [4]

Despite these compelling observations, the precise molecular mechanism underlying helix inversion in the 3-octyloxymethyl-substituted PQX induced by alkane solvents remains poorly understood. In the present study, we are trying a comprehensive investigation of the solvent-dependent helix inversion of a 100-mer PQX bearing (S)-3-octyloxymethyl side chains (**3oct**) in n-octane and cyclooctane. By performing SAXS, DLS, SANS and QENS experiments in conjunction with improved MD simulations.

EXPERIMENTS & RESULTS: Prior to the experimental investigations, molecular models of **3oct** were constructed using computational chemistry. Initially, the structures of the repeating monomeric units, comprising two conformational isomers (δ-monomer and λ-monomer), were optimized using the Forcite optimizer in BIOVIA Materials Studio 2024 with the COMPASS III force field at the ultra-fine level. Based on these optimized monomers, right-handed and left-handed 100-mer helical structures (P-δ-**3oct**, M-δ-**3oct**, P-λ-**3oct**, and M-λ-**3oct**) were constructed and further optimized. Currently, molecular dynamics (MD) simulations are being performed on each of these models under varying temperature conditions, and the results will be compared with those obtained from quantum beam scattering experiments.

REFERENCES:

(1) Nagata Y. *et al.,* J. Am. Chem. Soc., **135** (2013) 10104-10113.
(2) Nagata Y. *et al.,* J. Am. Chem. Soc., **140** (2018) 2722-2726.
(3) Inoue R. *et al.,* J. Chem. Phys., **161** (2024) 054905.
(4) Nagata Y. *et al.,* J. Am. Chem. Soc., **136** (2014)15901-15904.

CO4-15

Magnetic Measurements of Irons in Soda-lime Glass by Mössbauer Spectroscopy (3

K. Okada, and Y. Kobayashi[1]

SPring-8/JASRI
[1]Graduate School of Engineering, Kyoto University

INTRODUCTION: Glass is used in many applications in our every-day lives and has exciting new applications related to the energy. Soda-lime glass is made of mainly silica (SiO_2) and additive many other materials, such as magnesium, sodium, calcium, aluminum, iron, sulfur, and so on. Our reference glass composition, in percent by weight (wt%), was 72.25 SiO_2, 1.75 Al_2O_3, 4.00 MgO, 8.00 CaO, 14.00 Na_2O as basic components, and 0.015-5 iron in terms of Fe_2O_3 as coloring components. Iron contaminants of less than 0.0005-0.01 wt% from raw materials, and iron injection up to 1.5-5 wt%. We added compatible $CaCO_3$ and Na_2CO_3 as CaO and Na_2O, respectively. The iron oxides in a glass composition are thought to be present in forms of Fe^{3+} and Fe^{2+}. The control parameters for irons are two: (1) the total iron mass weight percent in terms of Fe_2O_3, and (2) the ratio of $Fe^{2+}$to total iron ions (Fe^{2+}/Σ_nFe). The Fe^{3+} component adds a light yellow tint to the glass and absorption in the ultraviolet and visible band, while the Fe^{2+} component adds a blue tint to the glass and absorption in the near-infrared band (1 μm). The transmission from ultraviolet to infrared in glass cannot be explained by simple Fe^{2+} and Fe^{3+} structures. Then, to reveal the exact local structures of irons (Fe^{2+} and Fe^{3+}) is necessary. Many scientists proposed many new theories and local structures [1-2], but they did not resolve it completely.

We have prepared reference glass samples with using the Mössbauer isotope ^{57}Fe (natural abundance is about 2.119 %) for measurements. The chemical composition of iron oxide in the ^{57}Fe enrichment glass was from 0.015 to 5 wt%, and the Fe^{2+}/Σ_nFe was from 0 to 0.6. We have investigated these samples by nuclear resonant inelastic scattering and XAFS methods at synchrotron radiation to reveal the local atomic structure around and neighboring iron atoms in sub-nanometer region [3].

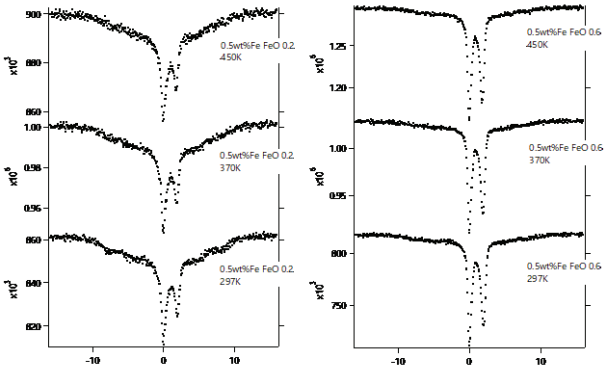

Fig. 1. Mössbauer spectra of the glass with 0.2 Fe^{2+}/Σ_nFe and 0.6 Fe^{2+}/Σ_nFe of 0.5 wt% alpha-Fe_2O_3. The measurements were performed at 297 K, 370 K, and 450 K.

EXPERIMENTS: We observed two samples with 0.2 Fe^{2+}/Σ_nFe and 0.6 Fe^{2+}/Σ_nFe of 0.5 wt% alpha-Fe_2O_3. The measurements were performed using conventional Mössbauer spectrometer at 297, 370, and 450 K. The specimens for Mössbauer measurements were tuned to 10 mm-phi pellet.

RESULTS: There were no difference between the three temperatures data with 0.2 Fe^{2+}/Σ_nFe and 0.6 Fe^{2+}/Σ_nFe of 0.5 wt% alpha-Fe_2O_3 as shown in Fig. 1.

REFERENCES:

[1] C. Ruessel *et al.,* Phys. Chem. Glasses, **47** (2006) 563.
[2] F. Farges *et al.,* Physica Scripta, **T115** (2005) 957.
[3] K. Okada *et al.,* X-ray Spectrometry, **47** (2018) 359-371.

CO4-16

Study on Resonant Frequency Change of Piezoelectric PZT with Radiation Irradiation

S. Takechi, S. Katayama, M. Okumoto[1], K. Nagasawa[1], S. Yamauchi[1], M. Kobayashi[2], T. Miyachi[2]

Graduate School of Engineering, Osaka Metropolitan University
[1]Department of Engineering, Osaka City University
[2]Planetary Exploration Research Center, Chiba Institute of Technology

INTRODUCTION: As a novel application of piezoelectric elements, we are exploring their use for radiation measurement. A key performance index of a piezoelectric element is the electromechanical coupling coefficient (k), which can be estimated from its resonance and anti-resonance frequencies. We found that the k value of a lead zirconate titanate (PZT) element, a type of piezoelectric material, changes when exposed to a 400 MeV/n Xe ion beam [1-3]. We are currently conducting electron beam irradiation experiments at the KURNS-LINAC to investigate how the k value of PZT elements changes under exposure to different types of radiation [4]. It is known that the k value of a PZT element decreases when the temperature exceeds a certain threshold. In FY2023, we investigated the changes in the k value of PZT element over several days under electron beam irradiation conditions, where the temperature was controlled to make the effects of temperature negligible. As a result, we found that the k value decreased monotonically with the cumulative dose of the 20 MeV electron beam and remained constant even after irradiation ceased [5].

EXPERIMENTS: The purpose of the experiment in FY2024 was to confirm the reproducibility of the experimental results obtained in FY2023 and to investigate the radioactivity of PZT due to irradiation. Experiments were conducted twice, in July and December 2024, each lasting three days, in which a PZT piezoelectric element was irradiated with an electron beam similar to that used in FY2023. The element is disk-shaped with a radius of 9 mm and a thickness of 1 mm, which was the same shape as in FY2023. The surface temperature of the PZT piezoelectric element during electron beam irradiation was monitored using a thermocouple. The electron beam irradiation time for each cycle was approximately 15 minutes. After the irradiation was stopped, the surface temperature of the PZT element was confirmed to be approximately at room temperature, and then the frequency-impedance characteristics of the element were measured. These measurements were performed 4 to 8 times per day. In the December experiment, after the frequency-impedance characteristics of the element had been measured, the radioactivity of the PZT piezoelectric element was measured for 10 minutes using an anti-Compton Ge detector.

RESULTS: After irradiating a PZT piezoelectric element with an electron beam for three days, we confirmed that the k value decreased monotonically with the increasing cumulative irradiation dose and that this decrease was sustained even after irradiation ceased. Gamma-ray measurements of the PZT piezoelectric element after electron beam irradiation, conducted using an anti-Compton Ge detector, revealed that the radioactive nuclides Pb-203 and Zr-89, which are isotopes of Pb and Zr—key constituent elements of PZT—were generated.

REFERENCES:

[1] M. Kobayashi *et al.*, Jpn. J. Appl. Phys., **52** (2013) 126604.
[2] M. Kobayashi *et al.,* Jpn. J. Appl. Phys., **53** (2014) 066602.
[3] S. Takechi *et al.,* Jpn. J. Appl. Phys., **60** (2021) 038003.
[4] S. Takechi *et al.,* Jpn. J. Appl. Phys., **61** (2022) 128001.
[5] S. Takechi *et al.,* Jpn. J. Appl. Phys., **63** (2024) 078002.

CO4-17

Positron Lifetime of β-$FeSi_2$ Film Probed by a Short-Pulsed Slow Positron Beam

A. Yabuuchi

Institute for Integrated Radiation and Nuclear Science, Kyoto University

INTRODUCTION: β-$FeSi_2$ is expected to be an environmentally friendly infrared light-emitting material. However, further enhancement of luminescence intensity is desired for practical applications. The Doppler broadening of annihilation radiation measurements using the KUR slow positron beam suggested that Al doping, which has been reported to enhance luminescence intensity, promotes the formation of Fe vacancies. In this study, positron annihilation lifetime measurements using the KUR slow positron beam were performed to investigate the size of atomic vacancies in β-$FeSi_2$ thin film.

EXPERIMENTS: A polycrystalline β-$FeSi_2$ film was fabricated on a Si substrate using the ion beam synthesis method. The positron annihilation lifetime of the film was measured using the KUR short-pulsed slow positron beam. The incident positron energy was determined to be 2 keV to probe the film region. In addition, yttria-stabilized zirconia (YSZ) single crystal, whose positron lifetime is well known [1], was also measured as a reference. The positron lifetime spectra obtained from the measurements were compared with simulated spectra based on the calculated positron lifetimes for β-$FeSi_2$ that have been reported [2].

RESULTS: The calculated positron lifetimes for defect-free β-$FeSi_2$ crystal, Fe monovacancy, and Si monovacancy have been reported as 137 ps, 172 ps, and 175 ps, respectively [2]. Figure 1 shows simulated positron annihilation lifetime spectra corresponding to these positron lifetimes. Figure 2 shows the positron annihilation lifetime spectra obtained from measurements of the reference YSZ and undoped β-$FeSi_2$. The measured positron lifetime for YSZ (179 ps) agrees with the reported value [1]. On the other hand, a positron lifetime component of 300 ps is observed from the positron lifetime measurements of the β-$FeSi_2$ film. This suggests the following possibilities: (i) vacancy clusters larger than monovacancies exist, or (ii) positrons are trapped at grain boundaries rather than within grains. Additionally, the possibility of influence from positron annihilation in the surface oxide layer cannot be excluded, as hydrofluoric acid treatment for oxide layer removal was not performed before measurement in this study.

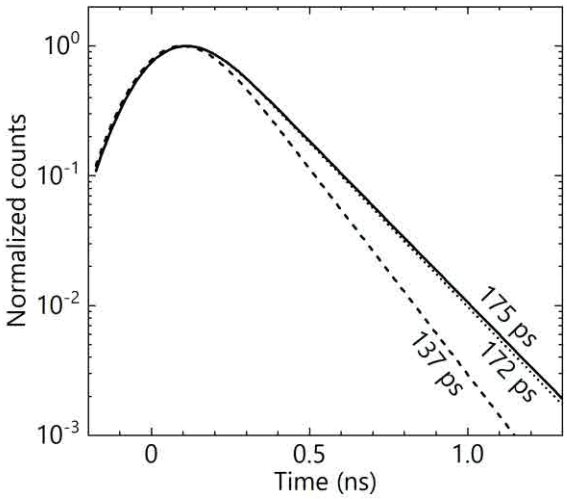

Fig. 1. Simulated positron annihilation lifetime spectra showing positron lifetimes of 137 ps, 172 ps, and 175 ps.

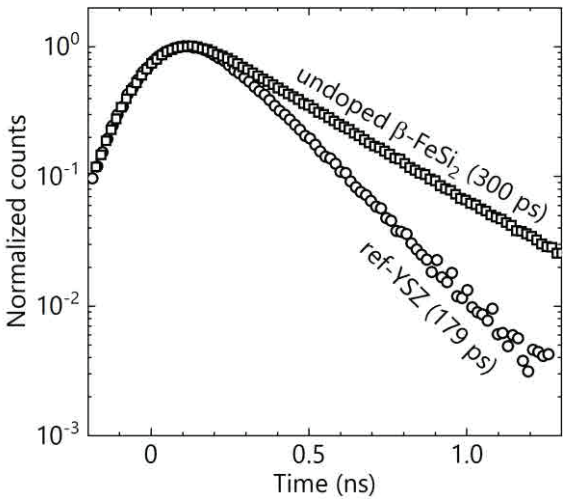

Fig2. Measured positron annihilation lifetime spectra of reference YSZ and the β-FeSi film.

REFERENCES: [1] O. Melikhova *et al.,* J. Phys.: Conf. Ser. **674** (2016) 012016.
[2] M. Mizuno, and H. Araki (2015) Chemical Bonding, Point Defects and Positron Lifetimes in $FeSi_2$ from First-Principles Calculations. In: T. Ishii, H. Wakita, K. Ogasawara, YS. Kim (eds) The DV-Xα Molecular-Orbital Calculation Method. Springer, Cham.

CO4-18

TDPAC Measurement of ^{111}Cd(←^{111}In) in Ultrafine Bubble Water

K. Takeshita, M. Tanigaki[1], A. Taniguchi[1], Y. Ueda[2], Y. Tokuda[3], and Y. Ohkubo[1]

Graduate School of Science, Kyoto University
[1] Institute for Integrated Radiation and Nuclear Science, Kyoto University
[2]Research Institute for Sustainable Humanosphere, Kyoto University
[3]Faculty of Education, Shiga University

INTRODUCTION: Ultrafine bubbles, the gaseous cavities with diameters less than 1 μm, have recently attracted much attention because of their multi-functionalities [1]. Fundamental studies on such multi-functionalities of ultrafine bubbles are not well extended because they are smaller than the wavelength of radiant rays. Following the previous study [2], we continue investigating the interface of ultrafine bubbles by the time differential perturbed angular correlation (TDPAC) of ^{111}Cd(¬ ^{111}In) to investigate the essential origins of its multi-functionality. This time, the pH dependence of $A_{22}G_{22}(t)$ was investigated over a much broader pH range than in the previous study.

EXPERIMENTS: Typical four-counter TDPAC measurements were performed for the 171-245 keV cascade in ^{111}Cd(←^{111}In) in oxygen water and water with oxygen-ultrafine bubbles. The average diameter and the density of the ultrafine bubbles were 200 nm, respectively. The aqueous solution of $^{111}InCl_3$ at pH 2 from Nihon Medi-Physics was added to each sample and adjusted to pH 4, 7, 8.5, 10, and 13 by dilution with the respective solvent [2]. The angular correlation term $A_{22}G_{22}(t)$ is given by:

$$A_{!!}\ G_{!!}\ (t) = \frac{2(N(180°,t) - N(90°,t)0}{N(180°,t) + 2N(90°,t)}$$

where N(90°, t) and N(180°, t) are the counting numbers at 90 and 180 degrees, respectively. The time-dependent term $G_{22}(t)$ for each sample was obtained by normalizing $A_{22}G_{22}(t)$ by the asymmetry parameter A_{22} of 171-245 keV cascade in ^{111}Cd.

RESULTS: Typically observed $A_{22}G_{22}(t)$ spectra for ^{111}Cd(←^{111}In) in oxygen ultrafine-bubble water and those in oxygen-saturated water are shown in Fig. 1. No significant difference was not found in the spectra of oxygen ultrafine-bubbles and oxygen-saturated water, and the spectra for pH 4, 7, 8.5 are consistent with those reported by Demille [3]. In the cases of pH 10 and 13, $A_{22}G_{22}(t)$ in both oxygen-saturated water and oxygen ultrafine bubble water show a characteristic pattern around 40 ns, suggesting the existence of a non-axial symmetric electric field gradient at In site, which could lead to new insights into the structure of In complex ions.

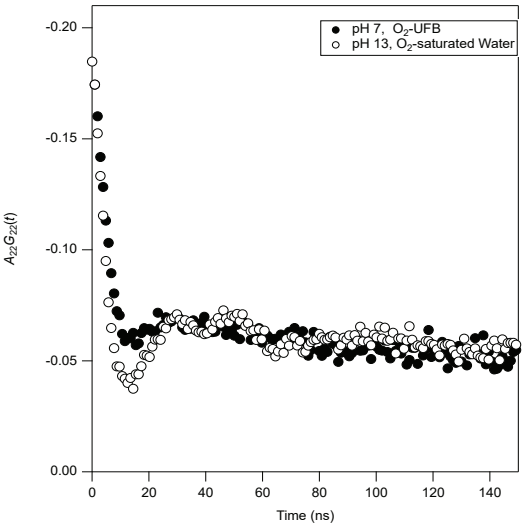

Fig. 1 Typical $A_{22}G_{22}(t)$ spectra of ^{111}Cd(←^{111}In) in oxygen ultrafine bubble water at pH 7 and in oxygen-saturated water at pH 13.

REFERENCES:

[1] E. G. Denis, "The fine bubble breakthrough," ISO News, 2014. Available: https://www.iso.org/news/2014/05/Ref1844.html.
[2] M. Tanigaki *et al.,* KURNS Progress Report 2023 (2024) 130.
[3] G. R. Demille *et al.,* Chemical Physics Letters, **44** (1976)164–168.

CO4-19

Fundamental study of damage on tungsten by heat and particle loading

K. Tokunaga, S. Akamaru[1], M. Matsuyama[1], Y. Hatano[2], M. Hasegawa, K. Nakamura and Q. Xu[3]

Research Institute for Applied Mechanics, KyushuUniversity
[1]Hydrogen Isotope Research Center, University of Toyama
[2]School y of Engineering, Tohoku University
[3]Institute for Integrated Radiation and Nuclear Science, Kyoto University

INTRODUCTION: It is of a great importance to clarify phenomena of implantation, retention, diffusion and permeation of tritium (T) on surface of the armor materials of the first wall/ blanket and the divertor on the fusion devices from a viewpoint of precise control of fuel particles, reduc-tion of tritium inventory and safe waste management of materials contaminated with tritium. In the present works, T exposure experiments have been carried out on tungsten (W) samples which were irradiated by high energy electrons and hydrogen beams to investigate effects of high energy elec-trons irradiation and high heat loading on microstructure and tritium retention of W. In this fiscal year, pure W were irradiated by repeated high energy negative hydrogen beams to investigate the effect of high heat loading of ELMs in fusion devises on T retention.

EXPERIMENTS: Stress relieved pure W (SR-W) has been exposed by multiple irradiations of a negative hydrogen ion beam with a energy of 3 MeV to investigate the influence of the repeated short pulse heat loading. After that, T exposure experiments on the exposed SR-W, non-irradiated SR-Ws and recrystallized W (RC-W) have been carried out using a T exposure device in University of Toyama. Pressure of the T gas was 1.3 kPa and T exposure was kept for 4 h at 100 °C. T concen-tration in the gas was about 5 %. After the exposure to T gas, T amount retained in surface layers of the samples was evaluated by imaging plate (IP) measurements and γ-ray-induced X-ray spectrom-etry (BIXS).

RESULTS: As shown in Fig. 1, microstructures of pure Ws are elongated to the roiling direction. After recrystallization, grain coarsening is generated and its sizes are almost the same. Microstruc-ture near the surface of H^- irradiated pure W changes to fine grains(B) and large grains (C) from rolling structure（A） as shown in Fig. 2. IP measurement after the T exposure indicates that T retention dependent on the microstructures as shown in Fig. 3. Distribution of T on cross section of the H^- irradiated pure W is now investigating.

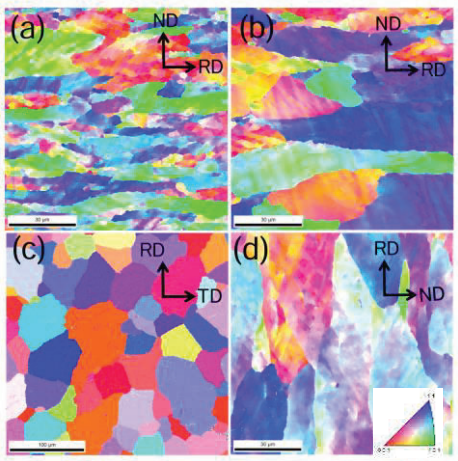

Fig. 1. IPF map (ND) (a)SR-W(PFW-672 TD), (b)SR-W(PFW-737 TD), (c)RC-W(ND), (d)SR-W(PFW-657-1 TD, H^--irradiated)

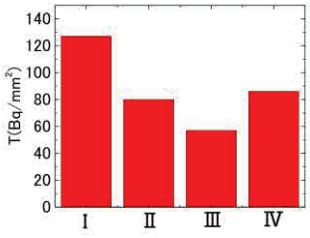

Fig. 3. Result of IP measure-ment Ⅰ, Ⅱ, Ⅲ and Ⅳ are (a), (b), (c) and (d) in Fig. 1

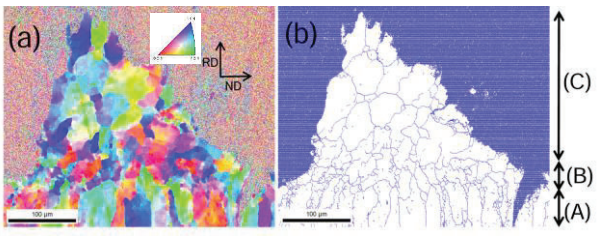

Fig. 2. Cross section near surface of H^- irradi-ated SR-W, (a) IPF map (ND), (b) RA(15°-180°)

CO4-20

Positron annihilation coincidence Doppler broadening of chromium oxynitride epitaxial films on magnesium oxide substrates

M. Kitaura, T. Sumi, A. Kinomura[1], M. Ishizaki, S. Watanabe[2], T. Suzuki[3]

Faculty of Science, Yamagata University
[1]*Institute for Integrated Radiation and Nuclear Science, Kyoto University*
[2]*Inovative Technology Laboratories, AGC Inc.*
[3]*Faculty of Engineering, Nagaoka University of Technology*

INTRODUCTION: Chromium oxide epitaxial films grown on magnesium oxide substrates have the rock salt structure of a cubic system,as same as the chromium nitride [1]. The hardness of this material is superior to that of the chromium nitride which is used as a hard coating film [2] . The chemical composition is Cr_2O_3, the same as the corundum structure of a trigonal system, and is different from that of chromium nitride (CrN). The chromium oxide epitaxial film is thus regraded as a defective rock salt structure with chromium-poor composition. Stacking faults of rock salt and corundum structures were found in chromium oxide epitaxial films. They occurred in chromium oxynitride epitaxial films with oxygen contents greater than 33%. The introduction of oxygens and chromium vacancies seems to be correlated with the formation of stacking faults in chromium oxynitride epitaxial films. So far, we have measured positron annihilation lifetimes of undoped and 3% oxygen doped CrN epitaxial films and chromium oxynitride epitaxial film with the oxygen content of 33% ($CrN_{0.67}O_{0.33}$) [3]. In the former two, positrons annihilated at the sites of chromium monovacancy. In the latter, the positron annihilation lifetime was drastically changed compared to the former two, but it remained unclear where positron annihilation occurs predominantly. In the present study, we have investigated positron annihilation Doppler broadening of CrN and $CrN_{0.67}O_{0.33}$ epitaxial films.

EXPERIMENTS: The sample of undoped and 3%O doped CrN and $CrN_{0.67}O_{0.33}$ epitaxial films were grown on MgO substrates by a pulse laser deposition method ion. The thickness was nearly 400 nm. It was confirmed that they have a cubic structure of the rock-salt type [3]. CDB experiments were performed at the slow positron beam line in KUR. The incident energy of the slow positron beam was set to 6 keV. The γ-ray photons emitted due to positron-electron pair annihilation were accumulated over 3 million counts.

RESULTS: Figure 1 shows CDB spectra of CrN and $CrN_{0.67}O_{0.33}$ epitaxial films on Mg substrates, which were obtained at 300 K. The integrated areas of the CDB spectrum were normalized to unity. The CDB spectra are almost the same between CrN and $CrN_{0.67}O_{0.33}$. Detailed analyses are currently underway.

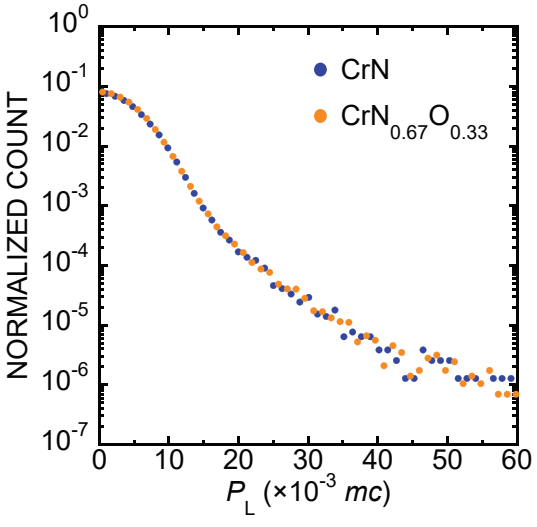

Fig. 1 CDB spectra of CrN and $CrN_{0.67}O_{0.33}$ epitaxial films.

REFERENCES:

[1] K. Suzuki *et al.,* APL Mater. **3** (2015) 096105.
[2] K. Suzuki *et al.*, Thin Solid Films **625** (2017) 111.
[3] M. Kitaura *et al.,* to be published from J. Phys.: Conf. Ser.

CO4-21

Research on radiation damage of new material (Ti high entropy alloy and industry steel (316L under and after irradiation

E. Wakai, A. Yabuuchi[1], T Yoshiie[2], K. Sato[3], T. Wakui, Y. Kobayashi[1], T. Takahashi[1], T. Ishida[4]

J-PARC Center, Japan Atomic Energy Agency
[1]Institute for Integrated Radiation and Nuclear Science, Kyoto University
[2]Department of Physics, Osaka Metropolitan University
[3]Research Field of Engineering, Kagoshima University
[4]J-PARC Center, High-Energy Accelerator Research Organization (KEK)

INTRODUCTION: Materials and instruments used in a radiation environment must have irradiation resistant properties. Therefore, it is important to promote research and development not only of existing applied and industrially developed materials, but alsoof innovative materials such as high entropy alloys [1,2] with even better properties. One of the objectives of this study is to understand the basic process of irradiation damage of high-entropy alloys as innovative materials. The electron-beam irradiation method, which can produce the simplest lattice defect, the Frenkel pair (energy must be adjusted), is an important experimental technique. Our efforts in this study have another objective. This is to detect the appearance of elastic waves produced by the stresses to which the material is subjected by the pulsed beam, and to measure and evaluate them using the four-terminal electrical resistance method as a nondestructive testing technique.

EXPERIMENTS: The electron irradiation experiments were performed using the electron linear accelerator at Kyoto University. In order to investigate the threshold energy of the atomic displacement process in Ti-64 (Ti-6Al-4V) alloy and Ti-based high-entropy alloys (Ti-V-Cr-Zn-Ta) caused by collisions with energetic incident particles, the temperature of the samples was kept at temperature about 4.0 K in a vacuum and the acceleration voltage of the electron beam was varied from 0.3 MV to 2.0 MV, and the electrical resistance of the sample was measured at each acceleration voltage by the four-terminal electrical resistance method [3]. Elastic waves excited in the 316L by pulsed electron beam waves (10, 20, 30, 50, and 100 Hz) around room temperature were also measured by the same 4-terminal electrical resistivity method in air at an energy of 8.0 MeV.

RESULTS: The electrical resistance of Ti-based HEA was found to change for the first time from at about 1.8 MeV, which is considered to be much higher than the generally assumed threshold energy of Ti alloys. This is an important result indicating the high threshold energy of this material and is an important factor in evaluating irradiation resistance performance. In the evaluation of the threshold energy of Ti-64 alloy, it was found to be higher than that of pure Ti. It was also evaluated to have a stepwise threshold energy. On the other hand, the results of the measurement by the 4-terminal electrical resistance method for elastic waves (stress waves) in solids induced by pulsed electron beams in the temperature region above room temperature were as follows. In 316L steel, the changes in electrical resistance tended to increase with increasing frequency (10-100 Hz). The results of this research and a detailed investigation of these material properties will be submitted to journals [4,5].

REFERENCES:

[1] E. Wakai *et al.,* Mater. Char., **211**(2024)113881.
[2] E. Wakai *et al.,* Sci. Talks, **8** (2023)100278.
[3] Y. Iwamoto *et al.,* J. Nucl. Mater., **458** (2015) 369-375.
[4] E. Wakai *et al.,* Advanced Mater. or Nature Com. or Materials Today to be submitted in 2025.
[5] E. Wakai or T. Wakai, *et al.,* Journal to be submitted in 2025.

CO4-22

Electrical Signals from Electron Device Measurement System under Irraditaion of Bremsstrahlung X-rays Produced by LINAC

Y. Gotoh, A. Kinomura[1], and T. Takahashi[1]

Graduate School of Engineering, Kyoto University
[1]Institute for Integrated Radiation and Nuclear Science, Kyoto University

INTRODUCTION: Electric and electronic circuits tolerant to radiation are important not only for decommissioning of Fukushima Daiichi Power Plant but also for the other nuclear power plants and radiation facilities [1]. To check the radiation tolerance, use of radioisotope (RI) is one of the good ways because radiation can be performed specific energy. Furthermore, RI does not cause electrical noise. However, it is rather difficult to observe individual event caused by the high energy particle, due to continuous radiation. To understand the events happening on electronic devices, its response after quick cease of the irradiation may give us some information. However, measurements of the electrical signals in radiation fields may have difficulties in acquiring such response from the device, due to the presence of unexpected noises. The purpose of the present study is to observe the response of the device together with electric noises produced in the measurement system under irradiation of Bremsstrahlung x-rays.

EXPERIMENTS: The samples were a silicon diode and an InGaP solar cell [2], which were installed in a small capsule made of stainless steel. Several samples were irradiated by pulsed X-rays generated by Bremsstrahlung of platinum target irradiated by 6 MeV electron beams. The output signal was taken out from the capsule via tri-axial cable. Current and voltage signals were acquired by a pico-ammeter and a digital oscilloscope. The pulse width was 4 μs and one pulse contained charges of 0.853 μC. Irradiations were performed at pulse repetition rates of 1 Hz and 60 Hz.

RESULTS: The ammeter detected little noise when the accelerator was not operated. Figure 1 shows a typical example of the voltage signal observed with the InGaP solar cell under x-ray irradiation. Rapid increase followed by a long tail, of which decay time was about several tens millisecond, was observed. The reason for the long decay time is currently unclear. The ammeter also recorded pulsed signal, and the observed pulse had also a longer time than the beam pulse. Further investigation will be necessary whether this method is applicable to extract some information on the effect of radiation to the electronic device, but the present InGaP solar cell may be used as a monitor of the beam pulse for low pulse repetition rate experiments.

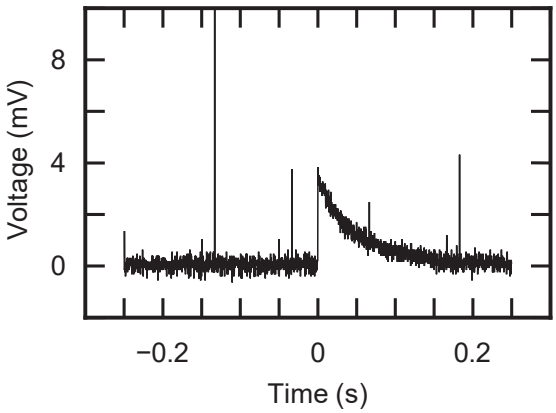

Fig. 1. Waveform of the X-ray induced signal obtained with an InGaP solar cell.

ACKNOWLEDGMENTS: The InGaP solar cells were provided by Dr. Mitsuru Imaizumi, Japan Aerospace Exploration Agency.

REFERENCES:
[1] Y. Gotoh *et al.,* IEEE Trans. on ED, **67** (2020) 1660-1665.
[2] Y. Okuno *et al.,* J. Nucl. Sci. Technol. **56** (2019) 851-858.

CO4-23

Vacancy Migration Energy in $CoCrFe_{0.25}MnNi$ High-Entropy Alloy

H. Araki, M. Mizuno, A. Yabuuchi[1] and A. Kinomura[1]

Graduate School of Engineering, Osaka University
[1]Institute for Integrated Radiation and Nuclear Science, Kyoto University

INTRODUCTION: Tsai et al. [1] originally proposed the concept of sluggish diffusion in the high-entropy alloy(HEA). However, the reason for the sluggishness of diffusion is not quite clear. $CoCrFe_{0.25}MnNi$ is known to form a quinary single-phased face-centered cubic structured solid solution. In the $CoCrFe_{0.25}MnNi$ HEA at high temperatures, atomic diffusion is expected to proceed via a vacancy mechanism because they are substitutional solid solutions. Therefore, vacancy formation and migration energies in the $CoCrFe_{0.25}MnNi$ HEA are important indexes for understanding the sluggish diffusion. In this work we have evaluated the vacancy migration energy in $CoCrFe_{0.25}MnNi$ HEA by observing the vacancy migration and annihilation behavior during an annealing process after electron irradiation, with the use of the positron lifetime spectroscopy.

EXPERIMENTS: An ingot of $CoCrFe_{0.25}MnNi$ HEA was carried out with solid solution heat treatment at 1373K for 24 h under argon atmosphere, and cut into 10 mm × 10 mm × 0.5 mm plates. The specimens were subjected to strain relief annealing at 1373K for 10 h and then rapidly cooled to prevent secondary phase precipitation and to stabilize single-phase FCC structure. Then, the specimens in water flow were exposed to 8 MeV electron beam irradiation for 3 h in KURNS-LINAC. The irradiation damage was evaluated at (1.3 - 1.8) $\times 10^{-4}$ dpa. The irradiated samples were isochronally annealed in a temperature range from 373 to 673 K. The temperature step during the isochronal annealing was 25 K and the duration of exposure to each temperature was 1 h. The positron lifetime measurements were made at 297–299 K.

RESULTS: Before the electron irradiation the positron lifetime spectrum for the solution-treated alloys was represented by only one component of 108 ps, which indicates that positrons annihilate in the bulk. After electron irradiation, the mean positron lifetime was increased to 132 ps. The analysis of positron lifetime spectra for the as-irradiated sample shows that many positrons are trapped and annihilate in the monovacancies introduced by electron irradiation, because the lifetime component, τ_2 , of trapped positrons was about 180 ps. The mean positron lifetime after isochronal annealing of the electron irradiated samples is shown in Fig.1. The mean positron lifetime is found to decrease sharply around 373K. This can be attributed to the decrease in vacancy concentrations triggered by the free vacancy-migration. It demonstrates the vacancy migration enthalpy in the $CoCrFe_{0.25}MnNi$ high entropy alloy is very similar to that in the CrFeNi alloy. These results indicate that the "'sluggish diffusion" hypothesis is not supported in $CoCrFe_{0.25}MnNi$ high entropy alloys at least in view of vacancy migration behavior.

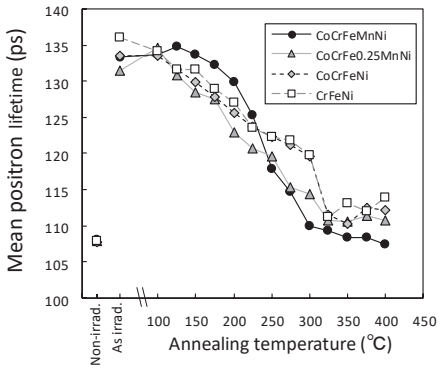

Fig. 1 Mean positron lifetime in the electron-irradiated $CoCrFe_{0.25}MnNi$ alloys after isochronal annealing.

REFERENCES:

[1] K. Y. Tsai, M. H. Tsai and J. W. Yeh, Acta Mater., **61** (2013) 4887.

CO4-24

Neutron Irradiation Tests for ITER Diagnostic Systems in JADA

T. Ushiki, K. Nojiri. T. Yokozuka, T, Kikuchi, S. Tainaka, E. Yatsuka, S. Kitazawa and Y. Nunoya

Department of ITER Project, Naka Institute for Fusion Science and Technology, National Institutes for Quantum Science and Technology

INTRODUCTION: ITER is the world's largest fusion experiment reactor and is under construction in southern France [1]. Components of diagnostic systems installed in the ITER tokamak are exposed to high neutron radiation. Therefore, it is important to investigate the effect of neutron irradiation on these components. In this study, neutron irradiation tests on components of ITER diagnostic systems in JADA (ITER project Japan Domestic Agency) have been conducted. This report presents the result of the neutron irradiation test on the optical fibers and electric devises for Infrared Thermography system (IRTh) [2] and pressure gauges for shutter on Divertor Impurity Monitor system (DIM), Edge Thomson Shattering system (ETS) and IRTh [3].

1. Irradiation test for IRTh

IRTh plans to use a steering mirror driven by an ultrasonic motor for optical axis adjustment in the ITER. A fiber optical rotary encoder and a precise limit switch are planned to be used for measuring the mirror angle and reference position. In this study, neutron irradiation tests on the fiber optical rotary encoder, optical fiber and limit switch were conducted.

EXPERIMENTS: The fiber optical rotary encoder, optical fiber and limit switch were irradiated at neutron fluence up to 1.0×10^{16} n/cm^2, equivalent to neutron fluences during 20 years of ITER operation. An evaluation of the transmittance at 800 nm, the use wavelength of the optical fiber, before and after irradiation, as well as functional tests of the fiber optical rotary encoder and the precise limit switch, were conducted.

RESULTS: It was confirmed that no significant degradation in transmittance was observed in the optical fiber before and after irradiation. Additionally, the precise limit switch was confirmed to function properly even after irradiation. The functional test of the fiber optical rotary encoder after irradiation is scheduled to be conducted around June 2025.

2. Irradiation tests of pressure gauges for shutter on DIM, ETS and IRTh

Pressure gauges are planned to be used on DIM, ETS and IRTh in the port cell area of ITER. Neutron irradiation tests on pressure gauges (K-P8AP) were performed to estimate neutron shielding that would last for 20 years ITER operation.

EXPERIMENTS: The irradiation position was outside of the graphite reflector in Slant Expose Tube (SLANT), and the thermal neutron flux at 5 MW operation was 4.8×10^{12} n/cm^2/s. The gauges irradiated up to 2.0×10^{12} n/cm^2 in the previous year were irradiated up to 3.0×10^{13} n/cm^2. The performance of the pressure gauge was compared before and after irradiations.

RESULTS: No change in the performance of the gauges was observed before and after the irradiation up to 3.0×10^{13} n/cm^2. The tested pressure gauges K-P8AP proved to be available at neutron fluence up to 1.0×10^{13} n/cm^2, equivalent to neutron fluences during 20 years of ITER operation.

REFERENCES:

[1] https://www.iter.org
[2] T. Ushiki *et al.,* J. Nucl. Mater., **595** (2024) 155047.
[3] K. Itami *et al.,* J. Plasma and Fusion Res., **92** (2016) 433.

CO4-25

Slow Positron Beam Analysis of Layered Structure Membrane

Z. Chen, Y. Kobayashi[1] A. Yabuuchi[2] and A. Kinomura[2]

Department of Material Science and Engineering, Wuhan Institute of Technology, People's Republic of China
[1]Department of Environmental Sciences, Tokyo Gakugei University
[2]Institute for Integrated Radiation and Nuclear Science, Kyoto University

INTRODUCTION: Membrane separation is an effective method for water treatment due to its low cost and low energy consumption [1]. Polyamide (PA) thin film composite membranes are widely studied owing to the tunable nature of their selective top layer and porous substrate. Since the thick selective layer may lead to the decrease of water flux, commercial composite membrane usually contains a thin selective layer. However, the defects in the thin selective layer would lead to serious decline of rejection, which is the main concern for membrane preparation. In order to solve the problem, introducing 2D material may be a potential method. Since the 2D material, such as $Ti_3C_2T_x$ (MXene), exhibits uniform nanochannels which is comparable to the ion size, PA/MXene/Polysulfone (PA/MX/PSF) layered structure may possess excellent performance. In this case, the PA/MX/PSF layered composite membranes have been prepared and investigated via positron annihilation techniques coupled with a positron beam.

EXPERIMENTS: The MXene aqueous solutions with different concentrations (0.03mg/L, 0.06mg/L, 0.12 mg/L and 0.18 mg/L) were filtrated by polysulfone membrane at 0.1 MPa, respectively. The piperazine (PIP) aqueous solution was poured on the surface of obtained MXene/polysulfone membrane for vacuum filtration. Then the trimesoyl chloride (TMC) was poured onto the obtained membrane surface for 1 min. The excess TMC solution was expelled after the PIP and TMC had reacted sufficiently to form the PA layer. Positron measurements were performed with the positron beam system at the Institute for Integrated Radiation and Nuclear Science, Kyoto University.

RESULTS: As shown in Fig. 1, the S-E curves of the four membranes suggested the difference of the layer structures. The S-E shape is similar to the positron results of PA/PSF membranes in the previous study [2]. In this study, all the four membranes are PA/MXene/PSF layered structure with different thickness of the MXene layer. Moreover, it can be found that thicker MXene layer would lead to the lower S parameter in the incident energies lower than 10 keV. The long-lived ortho-positronium (o-Ps) lifetime results at the incident energy of 1.65 keV and membrane rejections were shown in Table 1. It can be found that shorter o-Ps lifetime is corresponding to higher rejection. During the interface polymerization process, the existence of the MXene layer may hinder the loss of polymer monomer through porous substrate. In this case, thicker MXene layer may result in denser polyamide layer.

Table 1 The o-Ps lifetime and rejection of membrane

	o-Ps lifetime [ns]	Rejection of $MgSO_4$
PA/MX-3/PSF	2.17	70.1%
PA/MX-6/PSF	2.20	68.8%
PA/MX-12/PSF	2.16	81.1%
PA/MX-118/PSF	2.10	90.7%

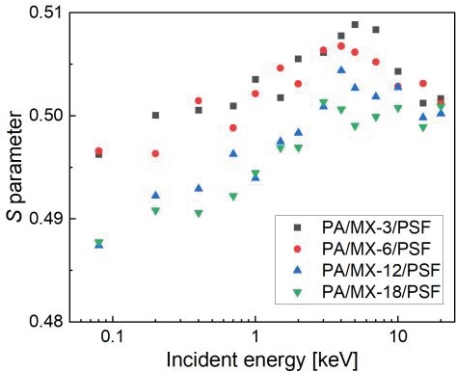

Fig. 1 The S-E plots for the samples.

REFERENCES:

[1] Y. Cui *et al.,* Water Research, **200** (2021) 117207.
[2] Z. Chen *et al.,* J. Phys. Chem. C, **115** (2011)18055-19060.

CO4-26

Changes in oxidation states of electrode material including Fe during discharging process

T. Wada and Y. Arachi
Department of Chemistry, Materials Engineering, Kansai University

INTRODUCTION: Oxide-based all-solid-state batteries (ASSBs) are expected to be the next-generation storage battery with both high energy density and chemical stability. Much research has been conducted on lithium metal as the anode. However, as the current density increases, there is a fatal problem that the precipitation of lithium metal in the sintered solid electrolyte leads to a short circuit between the electrodes. We believe that the anode of this battery requires an insertion electrode in which the charge/discharge reaction proceeds through the insertion and desorption reaction of Li ions into the crystal structure.

Electrochemical charge/discharge measurements confirmed that the charge/discharge reaction occurred at an average discharge voltage of 2.1 V in the first cycle, but the discharge capacity at the cutoff voltage of 1.8 V was only about 60% of the theoretical capacity (153 $mAhg^{-1}$), based on a one-electron reaction with Fe^{3+}. Furthermore, a significant capacity fading was observed toward the second cycle, and the reversible capacity gradually decreased with following cycles. Previous our research has shown that this material shows an ionic distribution of $[Li_{0.5}Fe^{3+}{}_{0.5}]^{8a}[Li_{0.25}Fe^{3+}{}_{0.25}Ti_{0.5}]^{16d}{}_2O_4$. Therefore, when Li is inserted into spinel-type $LiFeTiO_4$, it is possibly to change to rock salt-type Li_2FeTiO_4. In order to clarify the Fe oxidation state of the sample as well as the movement of Fe between sites (change in coordination environment) during charge/discharge reaction. For this purpose, we believe that Mössbauer spectroscopy is the most effective method.

EXPERIMENTS: The sample was prepared by conventional solid state reaction. As starting materials, Li_2CO_3, $FeC_2O_4 \cdot 2H_2O$ and TiO_2(anatase) were used and mixed by ball-milling for 30 min at 400 rpm and followed with sintering at 1273 K for 12 h in air. The obtained samples were charactered by powder X-ray diffraction and electrochemical testing. The electrode was treated by carbon-coating with acetylene black. As anode and electrolyte the lithium metal and 1 M $LiPF_6$ in EC-DMC (3:7) were used respectively.

RESULTS: A single cubic phase of the sample including Fe was confirmed by XRD pattern. Then the Rietveld refinement was carried out and yielded a relatively good fitting, based on the inverse spinel type structure. As shown in Fig. 1(1) and (4), both spectra showed magnetic splitting under trivalent Fe state. On the other hands, Fig. 1 (2) and (3) indicated an existence of divalent Fe, in addition to a small amount of trivalent one. These results can be explained by the electrochemical reduction reasonably. A further quantitative analysis are under progress to clarify the discharge and charging mechanism, focusing on local environment of Fe.

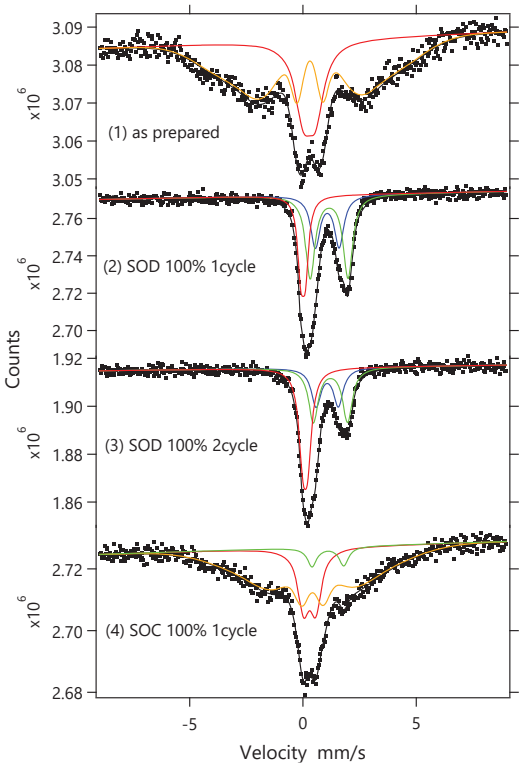

Fig. 1. ^{57}Fe Mössbauer spectra of various electrochemical oxidation states at 300 K. (1): as-prepared, (2): fully discharged at the first cycle, (3): fully discharged at the next 2nd cycle and (4) 1st cycled.

REFERENCES:

[1] Y. Arachi *et al.,* J. Jpn. Soc. Powder Powder Metallurg, **48(3)** (2001) 274-276.
[2] Y. Sakai, K. Ariyoshi and T. Ohzuku, Hyperfine Interactions, **139/140** (2002) 67-76.

CO4-27

Mössbauer spectrometric study of $SrTiO_3$ doped with dilute ^{57}Fe and Sn.

K. Nomura[1)], M. Takahashi[1)], Y. Kobayashi[2)], T. Naka[3)], Y. Yoshimura[4)], Y. Koike[4)], S. Kubuki[5)], J. Okabayashi[6)], and C. Barrero[7)]

[1] *Tokyo Medical University*
[2] *Institute for Integrated Radiation and Nuclear Science, Kyoto University*
[3] *National Institute of Material Science,*
[4] *Faculty of Science and Engineering, Meiji University,*
[5] *Radio-Isotope Center, Tokyo Metropolitan University,*
[6] *School of Science, The University of Tokyo,*
[7] *Faculty of Exact and Natural Sciences, University of Antioquia*

INTRODUCTION: Dilute magnetic semiconductors are required to have a Curie temperature above room temperature [1], and to achieve this, wide bandgap semiconductors doped with magnetic ions have been investigated [2]. In this study, we synthesized a strontium titanate ($SrTiO_3$: STO) doped with 1 at% $^{57}Fe^{3+}$ and several at% Sn^{4+} using a complexation/pyrolysis method. The local chemical states of iron were studied by Mössbauer spectrometry. At room temperature (RT), the two doublets due to the paramagnets and a broad relaxation peak were observed. The purpose is to clarify the origin of the broad peak by the low-temperature spectra.

EXPERIMENTS: The samples were prepared by the decomposition of the ethylene glycol complexes at 500 C for 2 hours and post-heating for 4 hours until 850 ºC. The formation of STO doped with 1 at% $^{57}Fe^{3+}$ and with and without several at% Sn^{4+} were mainly confirmed by XRD. VSM and SQUID measurements were carried out for 1 at% ^{57}Fe and 0–4 at% Sn samples.

RESULTS: We observed a very weak ferromagnetic behavior for 1 at% ^{57}Fe and 0−4 at% Sn co-doped samples. Mössbauer spectra of 1 at% ^{57}Fe doped and 1 at% ^{57}Fe + 4 at% Sn co-doped STO at RT, 200, and 75 K are shown in Fig. 1. The Mössbauer spectra of doped-STO at 75 K consist of four Fe^{3+} sites; two paramagnetic components and two magnetic relaxation components with different internal fields (about 50 and 20 T). Introducing Fe^{3+} and Sn^{4+} to Ti^{4+} sites can cause oxygen defects and lattice distortion. The ferromagnetic behavior can be attributed to the formation of clusters incorporating the oxygen vacancies, two Fe^{3+} atoms, and the strain-inducing Sn^{4+}. In some clusters, Fe^{3+} atoms achieved a long-range order [3].

REFERENCES:

[1] J.M.D. Coey *et al.,* Nature Materials, **172** (2005) 4.
[2] K. Nomura *et al.,* Hyperfine Interactions, **241** (2020) 6.
[3] A.M. Mudarra Navarro *et al.,* Interactions, **245** (2024) 21.

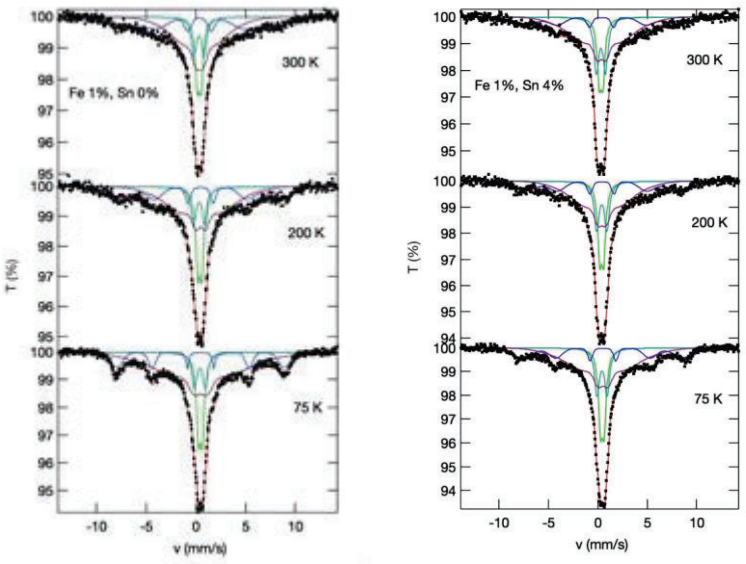

Fig. 1. Mössbauer spectra of 1% Fe doped STO (left) and 1%Fe +4%Sn doped STO (right) at 75, 200, and 300 K.